

Observation of subnatural-linewidth spectra in cold ${}^6\text{Li}$ atoms

Rui Li, Yuelong Wu,* Yang Rui, and Haibin Wu

Department of Physics, State Key Laboratory of Precision Spectroscopy, East China Normal University, Shanghai 200062, China



(Received 2 December 2020; accepted 1 February 2021; published 18 March 2021)

We report an observation of the subnatural-linewidth spectroscopy in cold ${}^6\text{Li}$ atoms by combining the interference contrast method and the time-delayed coincidence technique. The measured linewidth of D_1 lines is as narrow as 3.6 MHz, which is well below its natural linewidth of 5.8 MHz. The hyperfine splitting of the $2P_{1/2}$ state is measured as 26.112(20) MHz with this subnatural-linewidth spectroscopy. The transitions of the D_2 lines are partially resolved by using the developed technique. The time-delayed coincidence technique based on the interference contrast method in cold atoms provides a route for robust fluorescence measurements and determination of unresolved transitions.

DOI: [10.1103/PhysRevA.103.032823](https://doi.org/10.1103/PhysRevA.103.032823)

I. INTRODUCTION

Spectroscopy has been a key tool to understand the universe. It carries the information of atoms and molecules and plays an important role in many fields of physics, such as optical atomic clocks, tests of quantum electrodynamics, and measurements of fundamental constants [1–3]. The spectral resolution is typically determined by the natural linewidth, which is the result of quantum mechanics: A large number of atoms in an excited state decay photons statistically. In pursuit of improving the accuracy of the measurement, the sophisticated techniques have been developed to overcome this limitation. A narrower linewidth can be observed by detecting the fluorescence photons emitting at the time longer than the lifetime of atoms. Many previous works have developed various methods to improve the sensitivity of spectroscopy by selecting longer-lived atoms, such as Mössbauer spectroscopy [4–7], Ramsey resonance [8–10], and time-delayed coincidence [11–14].

Some previous measurements have been implemented in the thermal beams of alkali atoms, such as Na and Rb [15–18]. Lithium atoms are of particular interest among them. This is because due to their relatively simple three electronic structures, the accurate wave function and atomic structure can be obtained from the first principles, therefore, the high-precision lithium atomic laser spectroscopy has attracted great attention in the field of precision measurement [19,20]. However, because the hyperfine energy-level splitting of the D_2 line is smaller than the natural linewidth, it is difficult to resolve the transitions and, thus, hinders the improvement of the measurement. In this paper, we report an observation of subnatural-linewidth spectroscopy by combining the interference contrast method and the time-delayed coincidence technique in cold ${}^6\text{Li}$ atoms. The broadening mechanisms, such as Doppler broadening and collision broadening, are greatly suppressed by preparing the ultracold dilute atom sample (tens of microkelvin, lower than the Doppler cooling limit).

The spectroscopy is obtained by interfering the fluorescence photons between different delay times through phase switching of the probe light. The fluorescence photons emitting at the delay time larger than the lifetime of atoms are selected and detected. The linewidth of the D_1 line is narrowed to about 3.60 MHz, which is well below its natural linewidth of 5.8 MHz. With this observed subnatural-linewidth spectroscopy, the excited-state hyperfine splitting of the D_1 line is measured as 26.112(20) MHz, which agrees with the recent measurements [21]. The partially resolved spectroscopy of the D_2 lines is observed by using this technique. The result could be important to improve the accuracy of the transition frequencies of lithium atoms.

II. EXPERIMENTAL SETUP

The experimental setup is shown in Fig. 1, which is similar to our recent work in Refs. [21–23]. ${}^6\text{Li}$ is cooled from 673 K to 350 μK through a Zeeman slower and a standard magneto-optical trapping (MOT). Then, the gray molasses cooling is implemented to further reduce the temperature of atoms to 50 μK [24–27]. At this stage, 5×10^7 atoms with a 2-mm diameter of the cloud are prepared. The waist of the probe laser is chosen as 1 cm to ensure the homogeneous distribution of laser intensity at the location of the atoms. To minimize the atom number loss during the interaction, the probe laser intensity is attenuated to about $0.01I_{\text{sat}}$ ($I_{\text{sat}} = 7.5 \text{ mW/cm}^2$ is the saturation intensity of the D_1 lines). The scattered light by the atoms is collected by a large diameter lens and sent to a polarized maintained single-mode fiber in the direction perpendicular to the probe laser. The photons of the fluorescence is finally recorded by a commercial SPCM and processed by a FPGA at a time resolution of 10 ns. Each single experiment cycle takes 4 s, during which the phase of the probe laser is reversed for 30 times.

Figure 1(a) shows the schematic of the experimental setup. The probe laser at 671 nm is locked to a USC. The laser first double passes an AOM1, which is always kept on, and a small part of the laser light is used as the intensity feedback to control the power fluctuation of probe laser less than 2%

*ylwu@lps.ecnu.edu.cn

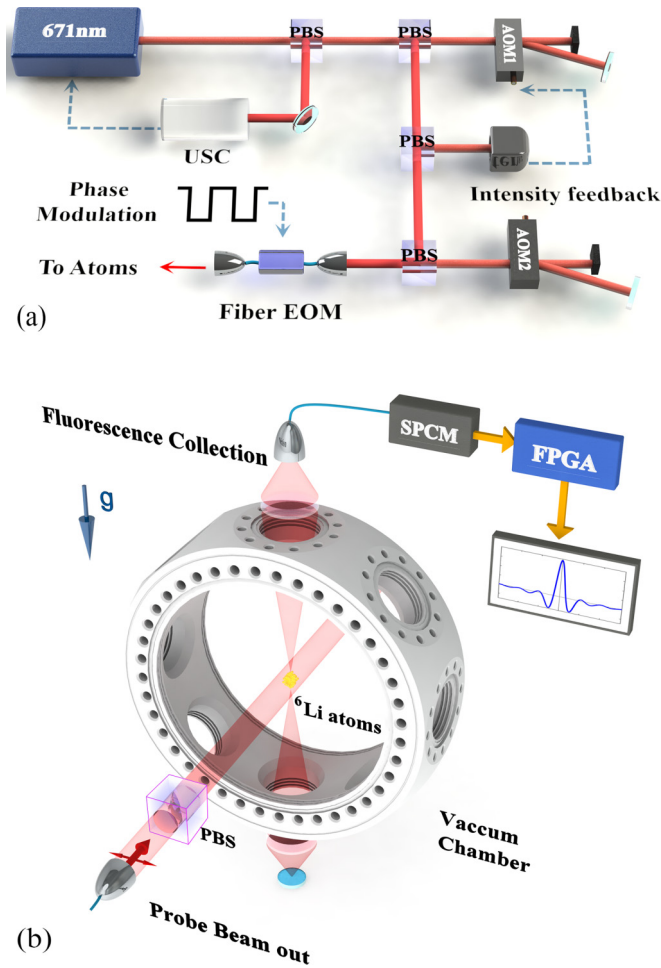


FIG. 1. Schematic of the experimental setup. (a) Probe laser system. The frequency of the probe laser is locked to an ultrastable optical cavity, and the frequency linear shift is better than 100 kHz per day. (b) Schematic of the fluorescence detection. Ultrastable cavity (USC); acousto-optic modulator (AOM); polarized beam splitter (PBS); single-photon counting module (SPCM); field programmable gate array (FPGA); electro-optic modulator (EOM).

during the following frequency sweep. AOM2 is controlled by a transistor-transistor logic signal to realize the fast switch of the probe laser power. A fiber-coupled EOM driven by a rapidly changing voltage signal is used to realize the fast phase switch of the probe laser. The time of phase switching is 5 ns which is limited by the response of the voltage turning over.

Figure 2 shows the timing sequence of the experimental process. After 3.5-s loading through the standard MOT, about 1.2×10^8 atoms at the temperature of 1 mK is obtained. Then, the cold atoms experience a compress stage. The Zeeman deceleration is turned off, and the detuning and intensity of the cooling and repumping laser are reduced whereas the magnetic-field gradient is increased from 10 to 20 G/cm during 10 ms. The temperature of the atoms is reduced to 350 μK with the number of atoms about 1.0×10^8 . Subsequently, the cooling repumping laser light and the magnetic field are turned off. Waiting for 500 μs is to avoid the residual magnetic field induced by fast switching of the coils. Then, the gray molasses of the D_1 line is implemented for 5 ms to further

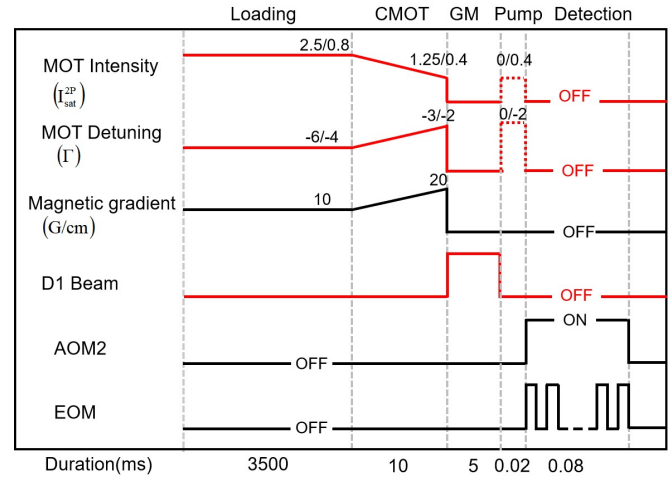


FIG. 2. Timing sequence of the probe process. There are five stages: loading, compressed MOT cooling (CMOT), D_1 gray molasses (GM), pump, and detection stages. AOM2 switches on/off the probe laser. The phase of probe laser is reversed by the fiber-coupled EOM for 30 times within a single measurement. The intensities and detunings of the cooling and repumping lasers are specified, respectively.

cool atoms to 50 μK with the number of atoms 5×10^7 . During the gray molasses cooling stage, the measured magnetic field at the interaction region is about 0.8 μT by the two-photon Raman spectroscopy. After the gray molasses cooling, a pump light is used to pump all the atoms to the $2S_{1/2}$, $F = 3/2$ state. The largest energy shift between different magnetic levels in the D_1 line under this residual magnetic field is 15 kHz. However, the imbalance of the population is just 0.56% from Boltzmann distributions. Therefore, the frequency shift due to the magnetic field is estimated to be 84 Hz.

After the cold atoms are prepared, the phase modulated weak probe laser is turned on to perform the detection of time-delayed coincidence. The fluorescence interference detection and the phase switch sequence are shown in Fig. 3. The green (upper) line represents the phase of the probe laser, the blue (bottom) square wave denotes two fluorescence collection windows, and the red (diagonal line) region shows the signal amplitude of the spontaneous emission. The data are collected in two windows for each measurement. Window1 receives the fluorescence only from the probe laser before the phase switching. Window2 receives the fluorescence from the probe laser both before and after the laser phase switching. Then, a SPCM is enabled in a 50-ns time window to record the fluorescence. The collected data are sent to a self-programmed coincidence apparatus based on FPGA for analysis. The phase of the probe laser is switched π after the first collection window, and the SPCM is enabled for a second 50-ns collection window. The interval between the second collection and the phase switching is a delay time t_d . After the two collection windows, the SPCM waits for 500 ns to start another measurement section. There are 30 sections for the measurement. The narrower linewidth can be obtained by increasing the value of t_d along with a fast decrease in the interference amplitude. The photons from two opposite directions are collected to increase the signal collection efficiency to 2% combined the coupling

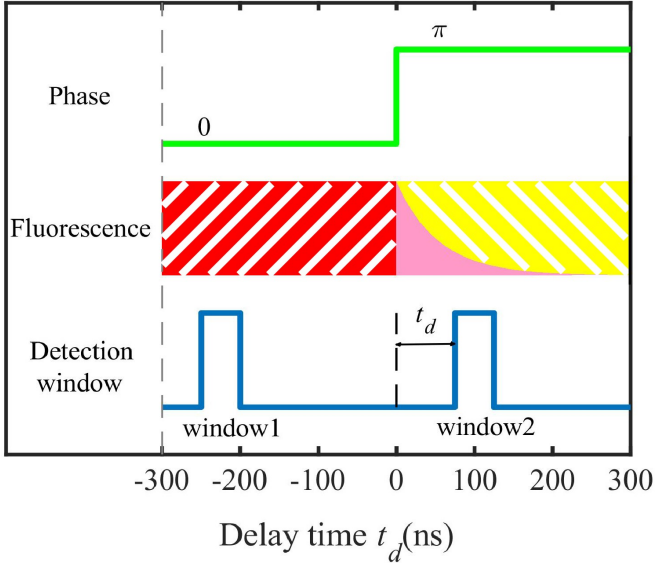


FIG. 3. The method of fluorescence interference detection, i.e., the detection stage in Fig. 2. The fluorescence is divided into three parts: the red region (antidiagonal line region) represents the fluorescence that the probe laser light with phase $\phi = 0$; the pink region (between the diagonal and the antidiagonal line region) represents the decay of fluorescence excited by laser light with the same phase $\phi = 0$; the yellow region (the diagonal line region) denotes for the fluorescence that the probe laser phase is reversed to $\phi = \pi$. Two of the many detection windows are shown here. The fluorescence excited by the probe laser with phase $\phi = 0$ is collected in the first window. The fluorescence that comes from laser light with $\phi = 0$ and $\phi = \pi$ are simultaneously detected in the second window where the interference signal is extracted to obtain the spectroscopy.

efficiency of the fiber 30%, and the overall fluorescence collection efficiency is about 0.6%.

III. THEORETICAL ANALYSIS

The time-delayed coincidence detection of fluorescence is to detect the interference signal between photons at different times, which can be understood by the model developed in Ref. [13]. In experiments, the probe laser intensity is kept constant. When the probe field E_0 is weak, the induced fluorescence $R(t_d)$ can be written as

$$R(t_d) = |E_0|^2 P_1(\Delta) + |E_0|^2 (e^{-i\phi} - 1) P_2(\Delta, t) + \text{c.c.}, \quad (1)$$

where ϕ is the phase, Δ is the frequency detuning between the probe laser and the atomic resonant frequency, γ_1 (γ_2), and γ_{12} are the decay rates of the excited-(ground-) state population and the coherence, c.c. is the complex conjugate,

$$P_1(\Delta) = \frac{\mu^2}{\hbar^2 \gamma_1 \gamma_2} \frac{1}{-i\Delta + \gamma_{12}}, \quad (2)$$

and

$$P_2(\Delta, t) = \frac{\mu^2}{\hbar^2 \gamma_2} \frac{e^{(i\Delta - \gamma_{12})t_d} - e^{-\gamma_1 t_d}}{(-i\Delta + \gamma_{12})(i\Delta - \gamma_{12} + \gamma_1)}, \quad (3)$$

respectively. The first term in Eq. (1) is denoted for the fluorescence signal of the steady-state response by the probe field after the phase switching. If the laser phase remains constant,

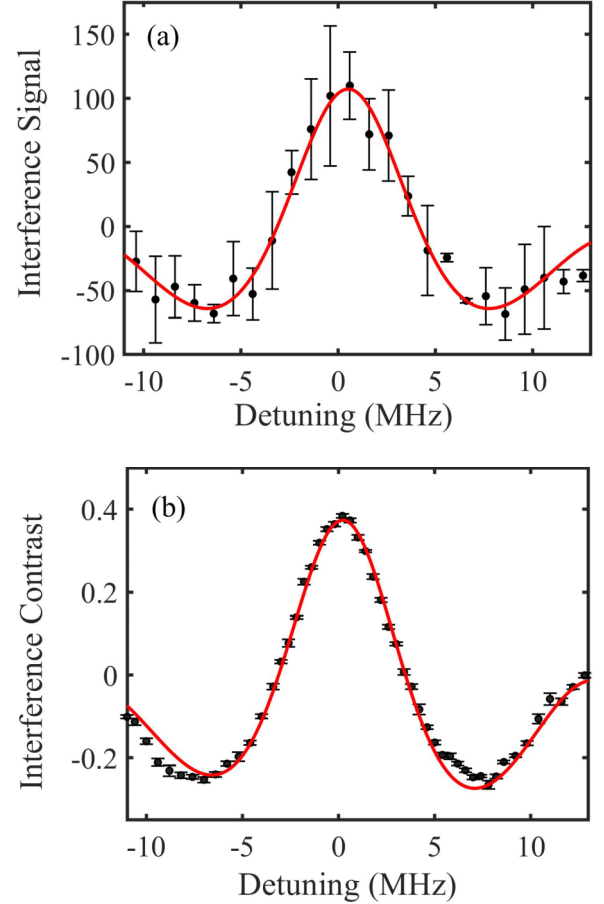


FIG. 4. The (a) interference signal and the (b) interference contrast signal of C_1 and C_2 at $t_d = 75$ ns. Here the detuning is denoted for the frequency difference of the probe laser relative to the transition $2S_{1/2}$, $F = 3/2 \rightarrow 2P_{1/2}$, $F' = 1/2$. Due to the fluctuation of the atom number from shot to shot, the signal-to-noise ratio (SNR) of the interference signal is only about 3.7. However, the SNR is improved to about 50 by using the interference contrast, and the statistical uncertainty is suppressed from 152 to 18 kHz. Error bars are the standard deviation (SD) of the repeat measurements.

i.e., $\phi = 0$, a normal fluorescence spectroscopy is obtained. The second term in Eq. (1) is the interference signal induced by phase modulation. In the experiment, the phase shift is adjusted to $\phi = \pi$. The photon counts in detected windows 1 and 2 can be expressed as

$$C_1 = A|E_0|^2 P_1(\Delta) + \text{c.c.}, \quad (4)$$

and

$$C_2 = A|E_0|^2 P_1(\Delta) - 2A|E_0|^2 P_2(\Delta, t) + \text{c.c.} \quad (5)$$

Counts C_1 and C_2 are linear to the atom number A . Count C_2 is the result of interference, which exponentially decreases with delay time t_d . The typical fluctuation of the atom number is about 10–20% from MOT to MOT [28,29]. For a large delay time exceeding 100 ns the interference intensity signal will be buried in the atom number noise. In order to improve the measurement, instead of the previous direct measurement of the interference intensity (photon counts) [11–14], here we use the interference contrast measurement

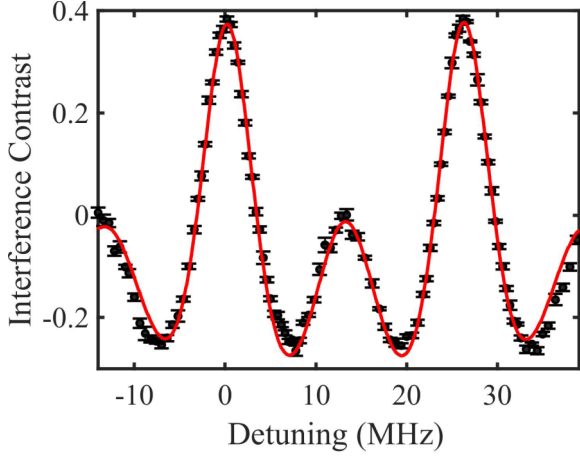


FIG. 5. The interference contrast of the transitions of $2S_{1/2}$, $F = 3/2 \rightarrow 2P_{1/2}$, $F' = 1/2, 3/2$ (left peak), $3/2$ (right peak). The delay time is $t_d = 75$ ns. The detuning is the frequency difference of the probe light relative to the transition $2S_{1/2}$, $F = 3/2 \rightarrow 2P_{1/2}$, $F' = 1/2$. The black dots are the measurement data of interference contrast for the average of five measurements with the same conditions. The error bars are the SD from statistics. The solid line is a fit based on the theoretical model. The measured splitting of the two peaks is 26.112(20) MHz.

[30,31] to make the measurement insensitive to atom number fluctuations. The interference contrast is defined as $\text{Con} = (C_1 - C_2)/(C_1 + C_2)$. As an example, the measured interference signal and interference contrast data as a function of Δ with $t_d = 75$ ns is shown in Fig. 4, the interference contrast data clearly gives better SNR, which makes the time-delayed coincidence measurement possible for longer delay time in cold atoms. Importantly, the fit residuals are greatly reduced from 13.5 to 1%, and the the statistics uncertainty is decreased from 152 to 18 kHz, which improves the following precision determination of the transition frequency.

IV. RESULTS AND DISCUSSION

In the experimental measurements, we first fix $t_d = 75$ ns and sweep the frequency of the AOM1 to obtain the spectroscopy of the D_1 line. A typical result of the transition $2S_{1/2}$, $F = 3/2 \rightarrow 2P_{1/2}$, $F' = 1/2, 3/2$ is shown in Fig. 5. The peaks corresponding to two transitions are clearly seen in the figure. The weak peaks located at about 15 MHz is a result of transient response of the coherent signal. The experimental data agree very well with a two-peak fitting based on the Eq. (1). The linewidth is 5.82 MHz (the linewidth is given by the full width at half maximum of the peaks). The hy-

TABLE I. ${}^6\text{Li}$ $2P_{1/2}$ hyperfine-structure intervals.

Splitting (MHz)	Reference
26.110(56)	[19]
26.111(15)	[20]
26.1031(14)	[29]
26.1026(6)	Theory [32]
26.112(20)	This paper

TABLE II. Uncertainty budgets (kHz) for the measurement.

Uncertainty component	D_1 lines
Reference frequency	0.6
Statistical variation	18
First-order Doppler	7
Magnetic field	0.084
Collision effect	<0.1
Local field effect	<0.03
Total	20.2

perfine interval is about 26.112(20) MHz, which agrees well with the recent measurements [19–21,32], see Table I for the comparison.

The measured uncertainties are shown in Table II. The dominant uncertainty is from the statistics of the data due to the fluctuation of the atom number from shot to shot and the reduced signal-to-noise ratio for the long delay time. The residual motion, the ballistic expansion of the atom cloud, and the acceleration by the probe beam are suppressed by the low temperature of the atoms after the gray molasses cooling. The local effect is greatly suppressed in our measurements

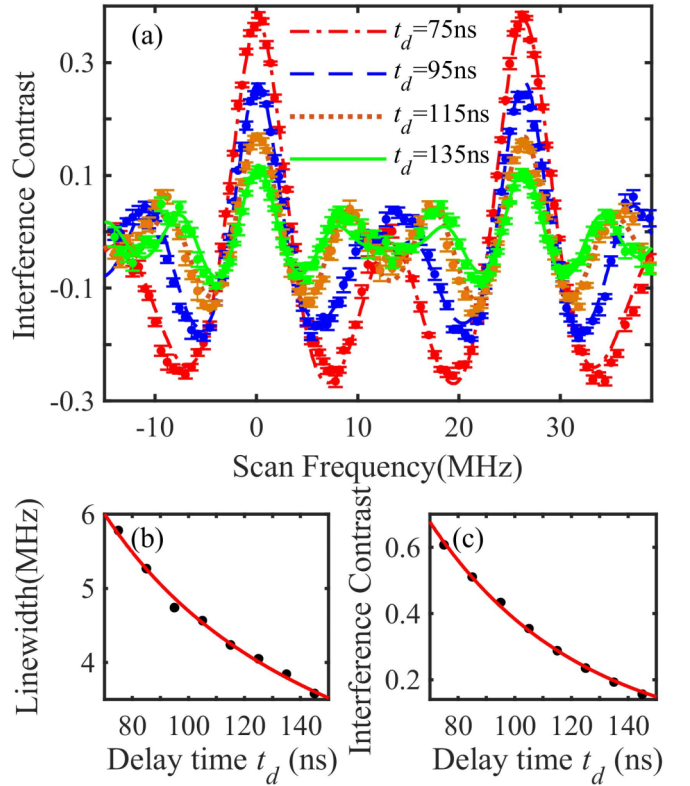


FIG. 6. (a) Subnatural-linewidth spectroscopy of the D_1 lines for the transitions of $2S_{1/2}$, $F = 3/2 \rightarrow 2P_{1/2}$, $F' = 1/2, 3/2$ (left peak), $3/2$ (right peak) with delay time $t_d = 75, 95, 115,$ and 135 ns. The detuning is the frequency difference of the probe light relative to the transition $2S_{1/2}$, $F = 3/2 \rightarrow 2P_{1/2}$, $F' = 1/2$. (b) The measured linewidths of the transition as a function of the delay time t_d . (c) The measured amplitude of the interference contrast as a function of the delay time t_d . The solid line is a fit with an exponential decay of Ae^{-bt_d} . The dots are the experimental data, and the solid lines are the theoretical fits. The error bars are from statistics.

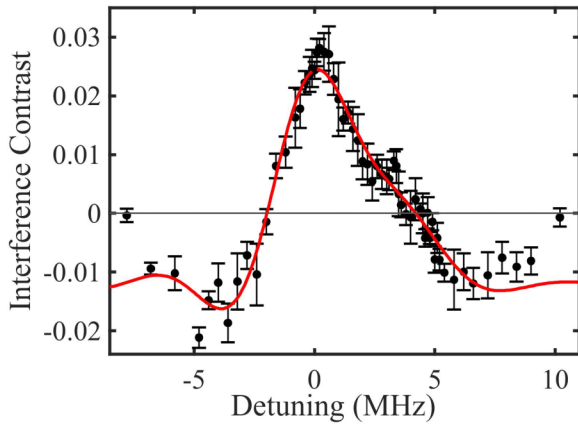


FIG. 7. Subnatural-linewidth spectroscopy of the D_2 lines for the transitions of $2S_{1/2}, F = 3/2 \rightarrow 2P_{3/2}, F'' = 5/2, 3/2, 1/2$. The delay time is $t_d = 200$ ns, and the spectroscopy linewidth is obtained about 3.5 MHz. The detuning is the frequency difference of the probe light relative to the transition $2S_{1/2}, F = 3/2 \rightarrow 2P_{3/2}, F'' = 5/2$. The dots are the experimental data, and the solid red line is the theoretical fit. The error bars are the SD from statistics.

due to very dilute atomic sample. Based on Refs. [33,34], the frequency shift from the local field effect $\Delta_{LL} = -\pi n_0 k^{-3} \Gamma$ is less than 30 Hz in our experiment, where n_0 is the atom number density, k is the wave vector, and Γ is the spontaneous emission rate. Other uncertainties are similar to our recent measurements [21].

The spectroscopy of the D_1 line with $t_d = 75, 95, 115,$ and 135 ns is shown in Fig. 6(a). The dots are the experimental data, and the solid lines are the theoretical fits. The linewidth as a function of t_d is plotted in Fig. 6(b). It is clear that the larger the delay time t_d , the narrower the linewidth. The linewidth fitting model is $\Delta\nu = 1/[2(t_d + t_0)] + f_0$, and t_0 counts for a small deviation in time due to the detection of the interference fluorescence of the delayed photons fallen in the collection windows. An offset f_0 is added to the fitting model for the residual broadenings where Doppler broadening take up a large part. For $t_d = 140$ ns, the linewidth is reduced to about 3.8 MHz. The dependence of the amplitude of the interference contrast on t_d is presented in Fig. 6(c). The amplitude fitting model is Ae^{-bt_d} . Although the spectral amplitude was decreasing with t_d , the SNR of the signal is still enough to obtain the subnatural-linewidth spectroscopy.

The same technique is used for the D_2 lines of ${}^6\text{Li}$. For the D_2 lines with the explicitly correlated Hylleraas basis [32], the energy splitting of $2P_{3/2}, F'' = 1/2 \rightarrow F'' = 3/2$ and $2P_{3/2}, F'' = 3/2 \rightarrow F'' = 5/2$ are 1.7118(12) and 2.8947(7) MHz, respectively. The hyperfine intervals are about 4.6 MHz, which is smaller than the natural linewidth,

and, therefore, they are very difficult to resolve. The optical spectroscopy with $t_d = 200$ ns for the transitions $2S_{1/2}, F = 3/2 \rightarrow 2P_{3/2}$ is shown in Fig. 7. The peaks are partially resolved. The red curve is the fit based on the interference contrast method. Since these transitions are partially resolved, quantum interference between the different excited hyperfine components has to be considered. By taking these effects into the fit, we obtained that the energy splittings of $2P_{3/2}, F'' = 3/2 \rightarrow F'' = 5/2$ and $2P_{3/2}, F'' = 1/2 \rightarrow F'' = 5/2$ are 2.75(10) and 3.86(20) MHz, which are 5% and 16% smaller than the most accurately predicted values, respectively. The difference may come from the fitting of complex quantum interference, the time-delayed coincidence, and the relatively low SNR. Although we can further increase the delay time to get a better resolution, the residual broadening and the small SNR set a limit for achieving the smaller linewidth in the real measurement. More powerful cooling techniques, such as evaporative cooling, are needed to further suppress the residual broadening of the spectroscopy.

V. CONCLUSION

We observe the subnatural-linewidth spectroscopy of cold ${}^6\text{Li}$ atoms. The time-delayed coincidence technique is used to select the photons emitting at the delay time longer than the lifetime of atoms, and, therefore, the linewidth of spectroscopy can be narrowed compared to the natural linewidth. The interference contrast method can improve the sensitivity of the measurements with long delay time t_d . By adjusting t_d , we obtained the ground-state hyperfine splitting as 26.112(20) MHz. The residual Doppler broadening of cold atoms limits the current linewidth to about 1 MHz. Higher-precision spectroscopy can be obtained by further reducing the temperature of atoms and increasing the fluorescence collection efficiency. It would be very useful to increase the SNR in the field of fluorescence measurement in cold atom systems and precision measurements of the transitions [35–38], especially, for transitions which are too close to be resolved.

ACKNOWLEDGMENTS

This research was supported by the National Key Research and Development Program of China (Grant No. 2017YFA0304201), the National Natural Science Foundation of China (NSFC) (Grants No. 11925401, No. 11734008, No. 11374101, and No. 12074125), the Shanghai Committee of Science and Technology (Grant No. 17JC1400500), the Shanghai Municipal Science and Technology Major Project (Grant No. 2019SHZDZX01), and the Innovation Program of Shanghai Municipal Education Commission (Grant No. 2019-01-07-00-05-E00079).

- [1] Th. Udem, R. Holzwarth, and T. W. Hansch, *Nature (London)* **416**, 233 (2002).
- [2] R. J. Rengelink, Y. van der Werf, R. P. M. J. W. Notermans, R. Jannin, K. S. E. Eikema, M. D. Hoogerland, and W. Vassen, *Nat. Phys.* **14**, 1132 (2018).
- [3] D. K. McKenzie and G. W. F. Drake, *Phys. Rev. A* **44**, R6973(R) (1991).

- [4] R. Grim, P. Gutlich, E. Kankleit, and R. Link, *J. Chem. Phys.* **67**, 5491 (1977).
- [5] P. Novak, J. Pechousek, V. Prochazka, J. Navarik, L. Kouril, P. Kohout, V. Vrba, and L. Machala, *Nucl. Instrum. Methods Phys. Res. Sect. A* **832**, 292 (2016).
- [6] D. W. Hamill and G. R. Hoy, *Phys. Rev. Lett.* **21**, 724 (1968).

- [7] R. N. Shakhmuratov and F. G. Vagizov, *Phys. Rev. A* **99**, 033831 (2019).
- [8] J. C. Bergquist, S. A. Lee, and J. L. Hall, *Phys. Rev. Lett.* **38**, 159 (1977).
- [9] M. M. Salour and C. Cohen-Tannoudji, *Phys. Rev. Lett.* **38**, 757 (1977).
- [10] R. Teets, J. Eckstein, and T. W. Hansch, *Phys. Rev. Lett.* **38**, 760 (1977).
- [11] F. Shimizu, K. Umez, and H. Takuma, *Phys. Rev. Lett.* **47**, 825 (1981).
- [12] H.-W. Lee, P. Meystre, and M. O. Scully, *Phys. Rev. A* **24**, 1914 (1981).
- [13] F. Shimizu, K. Shimizu, and H. Takuma, *Phys. Rev. A* **28**, 2248 (1983).
- [14] F. Shimizu, K. Shimizu, Y. I. Gomi, and H. Takuma, *Phys. Rev. A* **35**, 3149 (1987).
- [15] P. Juncar, J. Pinard, J. Hamon, and A. Chartier, *Metrologia* **17**, 77 (1981).
- [16] J. R. Brandenberger and R. E. Lindley, *Phys. Rev. A* **91**, 062505 (2015).
- [17] J. Wang, H. Liu, G. Yang, B. Yang, and J. Wang, *Phys. Rev. A* **90**, 052505 (2014).
- [18] W.-K. Lee and H. S. Moon, *Phys. Rev. A* **92**, 012501 (2015).
- [19] G. A. Noble, B. E. Schultz, H. Ming, and W. A. van Wijngaarden, *Phys. Rev. A* **74**, 012502 (2006).
- [20] C. J. Sansonetti, C. E. Simien, J. D. Gillaspay, J. N. Tan, S. M. Brewer, R. C. Brown, S. Wu, and J. V. Porto, *Phys. Rev. Lett.* **107**, 023001 (2011).
- [21] R. Li, Y. Wu, Y. Rui, B. Li, Y. Jiang, L. Ma, and H. Wu, *Phys. Rev. Lett.* **124**, 063002 (2020).
- [22] S. Deng, A. Chenu, P. Diao, F. Li, S. Yu, I. Coulamy, A. del Campo, and H. Wu, *Sci. Adv.* **4**, eaar5909 (2018).
- [23] S. Deng, Z. Shi, P. Diao, Q. Yu, H. Zhai, R. Qi, and H. Wu, *Science* **353**, 371 (2016).
- [24] D. R. Fernandes, F. Sievers, N. Kretzschmar, S. Wu, C. Salomon, and F. Chevy, *Europhys. Lett.* **100**, 63001 (2012).
- [25] A. T. Grier, I. Ferrier-Barbut, B. S. Rem, M. Delehay, L. Khaykovich, F. Chevy, and C. Salomon, *Phys. Rev. A* **87**, 063411 (2013).
- [26] A. Burchianti, G. Valtolina, J. A. Seman, E. Pace, M. De Pas, M. Inguscio, M. Zaccanti, and G. Roati, *Phys. Rev. A* **90**, 043408 (2014).
- [27] F. Sievers, N. Kretzschmar, D. R. Fernandes, D. Suchet, M. Rabinovic, S. Wu, C. V. Parker, L. Khaykovich, C. Salomon, and F. Chevy, *Phys. Rev. A* **91**, 023426 (2015).
- [28] S. Lee, K. Ravi, and S. A. Rangwala, *Phys. Rev. A* **87**, 052701 (2013).
- [29] M. Taglieber, A.-C. Voigt, F. Henkel, S. Fray, T. W. Hansch, and K. Dieckmann, *Phys. Rev. A* **73**, 011402(R) (2006).
- [30] F. V. Kowalski, W. T. Hill, and A. L. Schawlow, *Opt. Lett.* **2**, 112 (1978).
- [31] J. Mlynek, W. Lange, H. Harde, and H. Burggraf, *Phys. Rev. A* **24**, 1099 (1981).
- [32] M. Puchalski and K. Pachucki, *Phys. Rev. A* **79**, 032510 (2009).
- [33] J. Keaveney, A. Sargsyan, U. Krohn, I. G. Hughes, D. Sarkisyan, and C. S. Adams, *Phys. Rev. Lett.* **108**, 173601 (2012).
- [34] B. Zhu, J. Cooper, J. Ye, and A. M. Rey, *Phys. Rev. A* **94**, 023612 (2016).
- [35] L. Essen and J. Parry, *Nature (London)* **176**, 280 (1955).
- [36] L. Ma, Z. Bi, A. Bartels, L. Robertsson, M. Zucco, R. S. Windeler, G. Wilpers, C. Oatels, L. Hollberg, and S. A. Diddams, *Science* **303**, 1843 (2004).
- [37] A. D. Ludlow, M. M. Boyd, J. Ye, E. Peik, and P. O. Schmidt, *Rev. Mod. Phys.* **87**, 637 (2015).
- [38] W. Nagourney, J. Sandberg, and H. Dehmelt, *Phys. Rev. Lett.* **56**, 2797 (1986).